

Low-energy inelastic electron scattering from carbon monoxide: Excitation and de-excitation of the $X^1\Sigma^+$, $a^3\Pi$, $a'^3\Sigma^+$,$A^1\Pi$, $d^3\Delta$, $e^3\Sigma^-$, $I^1\Sigma^-$ and $D^1\Delta$ electronic states

Pengyu Wei(卫鹏宇), Chaowen Huang(黄朝文), XinluCheng(程新路), and Hong Zhang(张红)

Citation: Chin. Phys. B, 2024, 33 (**4**): 043101. DOI: 10.1088/1674-1056/ad123e
Journal homepage: http://cpb.iphy.ac.cn; http://iopscience.iop.org/cpb

What follows is a list of articles you may be interested in

Theoretical study of electron-impact broadening for highly charged Ar XV ion lines

Chao Wu(吴超), Xiang Gao(高翔), Yu-Hao Zhu(朱宇豪), Xiao-Ying Han(韩小英), Bin Duan(段斌),Ju Meng(孟举), Song-Bin Zhang(张松斌), Jun Yan(颜君), Yong Wu(吴勇), and Jian-Guo Wang(王建国)

Chin. Phys. B, 2023, 32 (**5**): 053101. DOI: 10.1088/1674-1056/acb769

Spectroscopy and scattering matrices with nitrogen atom: Rydberg states and optical oscillator strengths

Yuhao Zhu(朱宇豪), Rui Jin(金锐), Yong Wu(吴勇), and Jianguo Wang(王建国)

Chin. Phys. B, 2022, 31 (**4**): 043103. DOI: 10.1088/1674-1056/ac1f05

Effect of isotope on state-to-state dynamics for reactive collision reactions $O(^3P)+H_2^+ \rightarrow OH^+ + H$ and $O(^3P)+H_2^+ \rightarrow OH+H^+$ in ground state $1^2A''$ and first excited $1^2A'$ potential energy surfaces

Juan Zhao(赵娟), Ting Xu(许婷), Lu-Lu Zhang(张路路), Li-Fei Wang(王立飞)

Chin. Phys. B, 2020, 29 (**2**): 023105. DOI: 10.1088/1674-1056/ab6554

Theoretical study of the radiative decay processes in H^+(D^+, T^+)-Be collisions

Huilin Wei(魏惠琳), Xiaojun Liu(刘晓军)

Chin. Phys. B, 2018, 27 (**12**): 123101. DOI: 10.1088/1674-1056/27/12/123101

Stereodynamics of the reactions $Ne+H_2^+$ /$Ne+D_2^+$/$Ne+T_2$

Xiao Jing(肖静), Yang Chuan-Lu(杨传路), and Wang Mei-Shan(王美山)

Chin. Phys. B, 2012, 21 (**4**): 043101. DOI: 10.1088/1674-1056/21/4/043101

Low-energy inelastic electron scattering from carbon monoxide: Excitation and de-excitation of the $X^1\Sigma^+$, $a^3\Pi$, $a'^3\Sigma^+$, $A^1\Pi$, $d^3\Delta$, $e^3\Sigma^-$, $I^1\Sigma^-$ and $D^1\Delta$ electronic states

Pengyu Wei(卫鹏宇)[1], Chaowen Huang(黄朝文)[1], Xinlu Cheng(程新路)[1,†], and Hong Zhang(张红)[2]

[1] *Institute of Atomic and Molecular Physics, Sichuan University, Chengdu* 610065, *China*
[2] *College of Physics, Sichuan University, Chengdu* 610065, *China*

(Received 5 July 2023; revised manuscript received 29 November 2023; accepted manuscript online 5 December 2023)

Cross-sections for electronic excitation and de-excitation among the ground state and lowest-lying seven electronic excited states of carbon monoxide (CO) by low-energy electron impact are computed using the *R*-matrix method. The excitation cross-sections from the ground state to the electronic states $a^3\Pi$, $a'^3\Sigma^+$ and $A^1\Pi$ agree with previous experimental and theoretical results. In addition, the cross-sections for the $I^1\Sigma^-$ and $D^1\Delta$ states of CO, which will cascade to CO $a'^3\Sigma^+$ and $A^1\Pi$ states, are calculated. Furthermore, in contrast to the typical increase in electronic excitation cross-sections with collision energy, the de-excitation cross-sections show a negative trend with increasing energy.

Keywords: electron–CO collision, electronic excitation, cross-sections, *R*-matrix method

PACS: 31.15.A–, 52.20.Fs **DOI:** 10.1088/1674-1056/ad123e

1. Introduction

Accurate and reliable electron-impact cross-section data involving carbon monoxide (CO) are essential for informing spacecraft entry models in atmospheres akin to those found on Mars and Venus, as well as for investigating various atmospheric processes on these planets and in comets.[1] Furthermore, this data proves valuable in comprehending the mechanisms underlying CO laser operations and examining CO plasma behavior amidst electrical discharges.[2,3] Theoretical and experimental exploration of infrared emissions from CO in the upper atmospheres of Mars, Venus, and other celestial bodies remains an ongoing subject of interest.

Although the emission spectra of CO have been observed in numerous stars, the analysis and modeling of these spectra require more precise information about spectral assignment and cross-section. Over the past few decades, absolute cross-sections have been reported for the excitation and photoemission transitions of CO. However, there have been some significant discrepancies or even controversies arising from different experimental and data analysis methods.

Theoretical calculations on electronic excitation from the ground state of the CO molecule have been performed by several research groups. Chung *et al.* (1974) calculated the electronic excitation cross-sections of the $A^1\Pi$, $E^1\Pi$, $B^1\Sigma^+$, $C^1\Sigma^+$, $D^1\Delta$, $a^3\Pi$, $c^3\Pi$, $b^3\Sigma^+$, $j^3\Sigma^+$, $a'^3\Sigma^+$ and $d^3\Delta$ states of CO.[4] In a subsequent study, Sun *et al.* (1992) employed the Schwinger multichannel variational method with a fixed geometry and single-configuration representations of the target wavefunctions.[5] They investigated excitation cross-sections from the $X^1\Sigma^+$ state to the seven states $a^3\Pi$, $a'^3\Sigma^+$, $A^1\Pi$, $d^3\Delta$, $e^3\Sigma^-$, $I^1\Sigma^-$ and $D^1\Delta$ of CO within the collision energy range of threshold to 30 eV. Morgan *et al.* (1993) utilized the *R*-matrix method to compute electron-impact excitation cross-sections from the $X^1\Sigma^+$ state to the above mentioned seven lowest electronic states of CO within the energy range of 6 eV to 18 eV.[6] The results presented by Morgan *et al.* were derived from an eight-state model employing configuration interaction (CI) target wavefunctions (comprising the lowest eight states of CO, being $X^1\Sigma^+$, $a^3\Pi$, $a'^3\Sigma^+$, $A^1\Pi$, $d^3\Delta$, $e^3\Sigma^-$, $I^1\Sigma^-$ and $D^1\Delta$). Subsequently, Itikawa (2015) collected and reviewed cross-section data for electron collisions with CO, including total scattering, elastic scattering, momentum transfer, excitations of rotational, vibrational and electronic states, ionization and dissociation.[7] In Itikawa's study, the excitation cross-sections from the $X^1\Sigma^+$ state to the $a^3\Pi$, $a'^3\Sigma^+$, $b^3\Sigma^+$, $A^1\Pi$, $B^1\Sigma^+$, $C^1\Sigma^+$ and $E^1\Pi$ states are recommended for use. Recently, Zawadziki *et al.* (2020) performed a calculation using the *R*-matrix method to determine the differential and integral cross-sections of electronic excitation from the ground state to the $a^3\Pi$, $a'^3\Sigma^+$ and $A^1\Pi$ states of CO induced by electron collisions.[8]

As far back as 1971, Ajello systematically studied the CO spectrum using electron collision excitation and electron beam techniques, which impose stringent requirements on optical components and detection conditions, making it challenging to perform excitation cross-sections of the $A^1\Pi$ state through electron collision-induced fluorescence methods.[9] Therefore, in the 1990s, numerous research groups employed the energy loss spectrum method and performed integral cross-

†Corresponding author. E-mail: chengxl@scu.edu.cn

© 2024 Chinese Physical Society and IOP Publishing Ltd

sections (ICSs) through the measurement of CO differential cross-sections (DCSs). For instance, ICSs data were acquired using an indirect approach that measured the electron-impact excitation of the $a^3\Pi$ state. LeClair *et al.* and Furlong *et al.* performed experiments using various metastable detectors to investigate the phenomena described.[10,11] These experiments showed disagreement in the observed shapes above $E = 10$ eV and provided insight into the cascade processes that contribute to the $a^3\Pi$ state. Subsequently, extensive studies were carried out to fully explore the CO $A^1\Pi$ state, $a^3\Pi$ state, and other low-lying electronic states.

In general, direct electron collisions with diatomic molecules are considered inefficient due to the significant mass difference between electrons and molecules. However, when incident electrons can temporarily attach to form negative ions, the cross-sections for electronic (de-)excitation can be greatly enhanced.[12] Dora *et al.* performed resonance energies and widths of eight long-lived metastable electronic states of the CO^- anion as a function of bond distance using the *R*-matrix method.[13] Low-lying and broad $^2\Pi$ shape resonance is well known.

This study aims to investigate the electron-impact electronic excitation and de-excitation between the lowest eight electronic states ($X^1\Sigma^+$, $a^3\Pi$, $a'^3\Sigma^+$, $A^1\Pi$, $d^3\Delta$, $e^3\Sigma^-$, $I^1\Sigma^-$ and $D^1\Delta$) of CO in the low-energy region using the fixed-nucleus *R*-matrix method. In the following sections, we first present the electronic excitation cross-sections from the ground state to the above mentioned seven lowest electronic states and compare them with available experimental and theoretical results. We then analyze electron-impact electronic excitation cross-sections starting from the metastable excited states. To address the lack of data on electronic transitions between excited states of CO, we provide comprehensive data and a detailed analysis of the excited states, especially the $a^3\Pi$ triplet state and the $A^1\Pi$ singlet state.

2. Theoretical method

In this study, we used the well-established UKRmol+ code.[14] The use of mixed Gaussian *B*-spline basis functions to represent the continuum, target molecule orbitals provided by quantum chemistry algorithms such as Molpro,[15] enhanced configuration, which together with Hamiltonian generation are among the implementation's standout features. Below, we provide a brief discussion of the method; details of the principles involved can be found in the review article by Tennyson.[16]

The *R*-matrix method divides space into an inner region, where the physics is complex, and an outer region, where simplified equations can be solved. This division is achieved by employing an imaginary sphere, known as the *R*-matrix sphere, centered at the molecule's center of mass. The radius of the sphere is chosen so that it contains the entire wave function of the *N*-electron target states. In other words, the sphere's size is sufficiently large to ensure that all *N*-electron target states have zero amplitude at the boundary. In the inner region, where the collision complex is described by fully considering the exchange and correlation effects among all $N+1$ electrons, the resulting compound system behaves in a similar way to a bound state. Consequently, CI approaches, which have been developed for studying bound state problems, can often be extended to provide an *ab initio* treatment of the compound system, yielding the *R*-matrix on the boundary of the inner region. Inside the sphere, the $N+1$ electron scattering wavefunction ψ_k^{N+1} is represented by a close-coupling (CC) expansion using target state ϕ_i^N, given by

$$\begin{aligned}\psi_k^{N+1} &= A\sum a_{ijk}\phi_i^N(x_1\cdots x_N)u_{ij}(x_{N+1}) \\ &\quad +\sum b_{ik}\chi_i^{N+1}(x_1\cdots x_{N+1}),\end{aligned} \tag{1}$$

where the target contains N electrons and functions are labelled as N or $N+1$ according to whether they refer to the target or the compound scattering system, respectively. Here, $u_{ij}(x)$ are the continuum orbitals that represent the scattering electron. The operator A denotes the anti-symmetrization operation. The χ_i^{N+1}, called L^2 configurations, are performed by distributing all $N+1$ electrons among target molecular orbitals (MOs). The variational parameters a_{ijk} and b_{ik} are obtained from the diagonalization of the scattering Hamiltonian and are used in evaluating the *R*-matrix at the sphere boundary. The propagation of the *R*-matrix to large distances and matching with asymptotic solutions yields the reactance matrix (*K*-matrix). From the *K*-matrix, various quantities, such as the *T*-matrix, *S*-matrix and eigenphase, can be derived.

The *T*-matrices are in turn used to give a cross-section, σ, for going from target state i to target state i' using

$$\sigma(i\to i') = \frac{\pi}{k_i^2}\sum_S \frac{(2S+1)}{2(2S_i+1)}\sum_{\Gamma ll'}\left|T^{\Gamma S}_{ill'l'}\right|^2, \tag{2}$$

where $k_i^2/2$ is the energy of the scattering electron relative to the initial state, which has spin S_i. The first sum in Eq. (2) runs over the total number of spin states of the collision system, S, and the second sum runs over the spatial symmetries, Γ, and the degenerate channels associated with the initial and final target states, denoted l and l', respectively.

3. Computational details

Before starting scattering calculations, it is necessary to obtain the energies and wavefunctions. The MOs needed for the target and scattering calculations were performed with Molpro.[15] These calculations were carried out using the complete active space self-consistent field (CASSCF) method. The CASSCF calculation performed in this study is CAS(10,8),

wherein all ten valence electrons are distributed among the eight valence molecular orbitals, while the four core electrons remain frozen.

The target energies and vertical excitation energies performed from the CASSCF calculations are displayed in Table 1. Supplementary calculation results are also provided for comparative analysis, aiming to establish the credibility and precision of our calculations in support of subsequent research endeavors. Our results are compared with the theoretical results of other researchers, namely, Sun *et al.*[5] who employed the Schwinger multichannel variational method, Morgan *et al.*,[6] Dora *et al.*[13] and Zawakzki *et al.*[8] who utilized the *R*-matrix method, as well as the experimental values derived by Nielsen *et al.*[17] and Tilford *et al.*[18] It is evident that our results demonstrate better agreement with the experimental values than Sun *et al.* Furthermore, our results acquired with the cc-pVQZ Gaussian type orbital (GTO) basis set are marginally lower than those reported by Morgan *et al.*, primarily because Morgan *et al.* utilized Slater-type orbital (STO) to generate MOs. Moreover, our calculations marginally outperform Dora *et al.*, where the target MOs used in scattering calculations were acquired with Molpro state-averaging complete active space self-consistent field (SA-CASSCF) calculations. The vertical excitation energies of the $a^3\Pi$, $a'^3\Sigma^+$ and $A^1\Pi$ states are compared to those of Zawakzki *et al.* in Table 1, and our present study yields superior results. In general, the current vertical excitation energies are slightly higher than the experimental results, which is anticipated given that the experimental values account for the relaxation of the nuclei upon excitation.

Table 1. Target energies in Hartree for the ground state and vertical excitation energies in eV for the twelve excited states of CO, calculated using the cc-pVQZ basis set.

State	Present	Sun	Morgan	Dora	Zawakzki	Expt.[1]	Expt.[2]
$X^1\Sigma^+$	−112.8638098	–	–	–	–	–	–
$a^3\Pi$	6.46	6.00	6.43	6.43	6.77	6.32	6.32
$a'^3\Sigma^+$	8.50	7.94	10.03	8.36	8.97	8.50	8.51
$A^1\Pi$	9.11	9.71	9.12	8.97	9.46	8.58	8.51
$d^3\Delta$	9.33	8.84	9.74	9.22	–	9.34	9.36
$e^3\Sigma^-$	9.71	9.52	10.19	9.60	–	9.86	9.88
$I^1\Sigma^-$	10.05	9.71	10.31	9.95	–	10.01	9.88
$D^1\Delta$	10.08	10.14	10.37	10.00	–	10.12	10.23
$2^3\Sigma^+$	12.49	–	–	10.39	–	–	10.40
$2^3\Pi$	12.55	–	–	11.34	–	–	–
$2^1\Sigma^+$	13.29	–	–	11.16	–	–	–
$2^1\Pi$	14.17	–	–	11.84	–	–	–
$3^3\Pi$	14.93	–	–	12.32	–	–	–

For the scattering calculations, we utilized the UKRmol+ code[14] and the radius of the *R*-matrix sphere is set to $10a_0$. We acquired complete sets of MOs, including both occupied and virtual orbitals, with CASSCF calculations with a cc-pVQZ GTO basis set. The CC expansion included thirteen target states, namely, the $X^1\Sigma^+$, $a^3\Pi$, $a'^3\Sigma^+$, $A^1\Pi$, $d^3\Delta$, $e^3\Sigma^-$, $I^1\Sigma^-$, $D^1\Delta$, $2^3\Sigma^+$, $2^3\Pi$, $2^1\Sigma^+$, $2^1\Pi$ and $3^3\Pi$ electronic states. The electronic structures primarily arise from the following electronic configurations, as presented in Zobel *et al.*[19]

$$X^1\Sigma^+ \text{ (ground)}:$$
$$(1\sigma)^2(2\sigma)^2(3\sigma)^2(4\sigma)^2(1\pi)^4(5\sigma)^2,$$
$$A^1\Pi,\ a^3\Pi \text{ (valence)}:$$
$$(1\sigma)^2(2\sigma)^2(3\sigma)^2(4\sigma)^2(1\pi)^4(5\sigma)^1(2\pi)^1,$$
$$a'^3\Sigma^+,\ D^1\Delta,\ d^3\Delta,\ I^1\Sigma^-,\ e^3\Sigma^- \text{ (valence)}:$$
$$(1\sigma)^2(2\sigma)^2(3\sigma)^2(4\sigma)^2(1\pi)^3(5\sigma)^2(2\pi)^1.$$

The orbital energy calculations by Huo determined the order of the orbitals for the ground state of CO, with increasing energy leading to the configuration $1\sigma^2 2\sigma^2 3\sigma^2 4\sigma^2 1\pi^4 5\sigma^2$.[20] To represent the scattering electron, we utilized continuum orbitals generated by fitting the GTO basis sets to Bessel functions with $l \leq 4$.[21] The resonance positions and widths were determined and digitized by fitting the eigenphase sum calculated by EIGENP in the RESON module of the UKRmol+ code.[14]

The positions (E_r) and widths (Γ) of the resonances detected for CO at its equilibrium geometry, $R_{eq} = 1.1282$ Å, are provided in Table 2. The lowest-lying $^2\Pi$ resonance is well known from many experiments and theoretical calculations. In our calculation, the position of this resonance is found by RESON to be at 2.13 eV with a width of 0.95 eV. Most of the experiments report the position of this resonance to be at 1.6 eV. We can explain this error on the basis that the *R*-matrix method relies on the difference between the target and scattering state energies. Apart from a shape resonance $^2\Pi$, six Feshbach resonances at higher energy are identified. However, in this article, we do not emphasize the description of Feshbach resonance states.

Both Molpro and UKRmol+ are unable to utilize the natural $C_{\infty v}$ symmetry of the CO molecule. As a result, we performed these calculations using the reduced C_{2v} point group. However, since there are clear correlations linking electronic states between these two-point groups, we present the target and resonant states using $C_{\infty v}$ symmetry.

Table 2. Positions (E_r) and widths (Γ) of resonances detected for CO at its equilibrium geometry, $R_{eq} = 1.1282$ Å. All quantities are in eV.

Symmetry	E_r	Γ
$1^2\Pi$	2.1329774	0.94660925
$2^2\Pi$	11.039355	1.6634989
$3^2\Pi$	12.263467	1.9012801
$4^2\Pi$	11.512136	2.1452576
$5^2\Pi$	17.982766	0.34818786
$1^2\Sigma^-$	13.019448	4.129150
$2^2\Sigma^-$	17.362537	1.4517372

4. Results and discussion

4.1. Ground state

This section focuses on the electronic excitation cross-sections originating from the CO ground state. The present results are compared with previous measurements and theoretical data, where available. Figure 1 displays the electronic excitation cross-sections from the CO ground-state transition to seven excited states. The excitation cross-sections shown in Figs. 1(a)–1(c) are compared with experimental values fitted by Ajello,[9] Zobel *et al.*,[19] Zawakzki *et al.*,[8] the recommended values by Itikawa[7] in his review article, and the theoretical data from the *R*-matrix method by Zawakzki *et al.*[8]

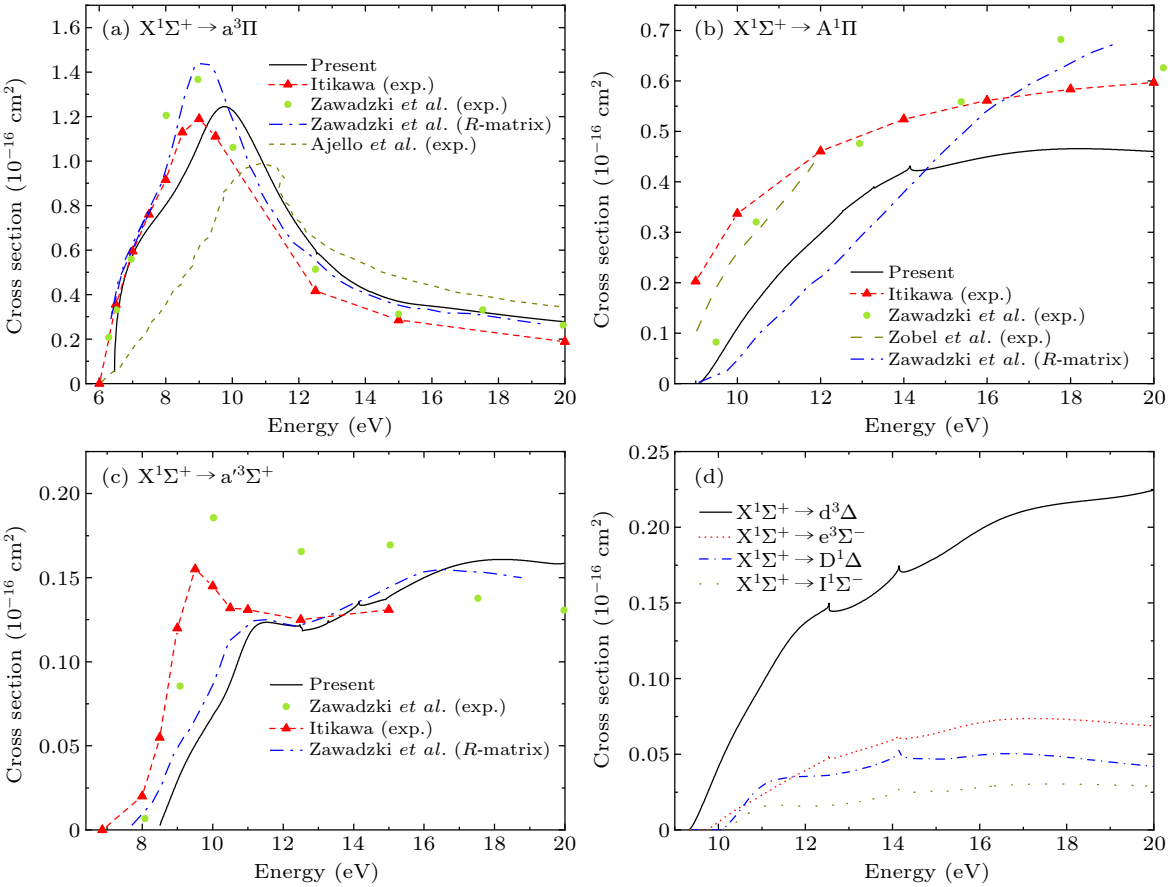


Fig. 1. Electronic excitation cross-sections from the CO ground state $X^1\Sigma^+$ transition to the seven excited states.

The cross-section maxima performed from our calculations show similarity to the cross-section maxima reported by Itikawa in the electronically excited transition of $X^1\Sigma^+ \rightarrow a^3\Pi$. Furthermore, upon analyzing the electronically excited transition of the $X^1\Sigma^+ \rightarrow A^1\Pi$, the trend of our graphic shape agrees with that of experimental data. In the case of $X^1\Sigma^+ \rightarrow a'^3\Sigma^+$, although the results acquired by Zawakzki *et al.* (*R*-matrix) are in closer agreement with the experimental values, there exists minimal variance between our results and those of Zawakzki *et al.* (*R*-matrix). The reason for the variances is that Zawakzki *et al.* (*R*-matrix) employed the large cc-pV6Z Gaussian basis set. In contrast, we utilize the cc-pVQZ Gaussian basis set. When deriving the ICSs in experimental calculation, it was necessary to extrapolate the DCSs to account for missing angles, which introduces uncertainty into the theoretical data results.

This comparison between our study and prior research implies that the calculated excitation function for CO, in terms of both magnitude and shape, is plausible within the energy range considered. Consequently, we can assert that the model provides a precise description of excitation cross-sections at low energies. As a result, we employ this model to compute electron scattering with the $d^3\Delta$, $e^3\Sigma^-$, $I^1\Sigma^-$ and $D^1\Delta$ excited states of CO. The corresponding calculated ICSs for the $d^3\Delta$, $e^3\Sigma^-$, $I^1\Sigma^-$ and $D^1\Delta$ states are depicted in Fig. 1(d). The local maximum cross-section values for these $X^1\Sigma^+ \rightarrow e^3\Sigma^-$ and $X^1\Sigma^+ \rightarrow d^3\Delta$ two processes occur at the energies of 12.47 eV and 14.15 eV, respectively. Furthermore, the cross-section values for $X^1\Sigma^+ \rightarrow d^3\Delta$ transitions are greater than those of other processes.

4.2. Metastable excited states

4.2.1. The $a^3\Pi$ state

Ajello proposed potential band systems that might undergo a cascade to the $a^3\Pi$ state, including $a'^3\Sigma^+ \rightarrow a^3\Pi$ and $d^3\Delta \rightarrow a^3\Pi$.[9] Leclair *et al.* demonstrated this cascade phe-

nomenon by observing that the time-of-flight spectrum of the CO $a^3\Pi$ state shows a significantly longer lifetime than these high triplets ($a'^3\Sigma^+$, $d^3\Delta$ and $e^3\Sigma^-$).[10] However, it is not possible to determine from the excitation cross-section data whether a cascade onset occurs. To address this, we employ the *R*-matrix method to calculate the magnitude of the cascade based on the excitation cross-sections. The analysis reveals that the cascade contributions are indeed substantial. This increases our understanding of experimental errors when the electron beam excitation experiment method is used to study the Cameron system ($a^3\Pi \rightarrow X^1\Sigma^+$) of CO.

As depicted in Fig. 2(a), the cross-sections for de-excitation of the $a^3\Pi \rightarrow X^1\Sigma^+$ decrease as the incident electron energy increases. The ICSs for de-excitation display an initial rapid decrease, followed by a gradual decline. A very distinct peak structure for the electronic transitions $a^3\Pi \rightarrow A^1\Pi$ exists at 11.40 eV. We performed calculations to determine the cross-sections for transitions from the $a^3\Pi$ state to the $a'^3\Sigma^+$, $d^3\Delta$, $e^3\Sigma^-$, $I^1\Sigma^-$ and $D^1\Delta$ higher states of CO, as shown in Fig. 2(c). The excitation cross-sections for $a^3\Pi \rightarrow a'^3\Sigma^+$ show a maximum peak around 10.36 eV. The electronic transitions of $a^3\Pi \rightarrow d^3\Delta$ and $a^3\Pi \rightarrow a'^3\Sigma^+$ show similar shapes and magnitudes. The electronic transitions of $a^3\Pi \rightarrow d^3\Delta$ reach a maximum value of 0.149 Å^2 at 11.50 eV. In contrast, the cross-sections for the electronic transition of $a^3\Pi \rightarrow e^3\Sigma^-$, $I^1\Sigma^-$ and $D^1\Delta$ do not exceed 0.052 Å^2. The electronic transitions shown in Fig. 2(c) all have two peaks, occurring at approximately 12.54 eV and 14.15 eV.

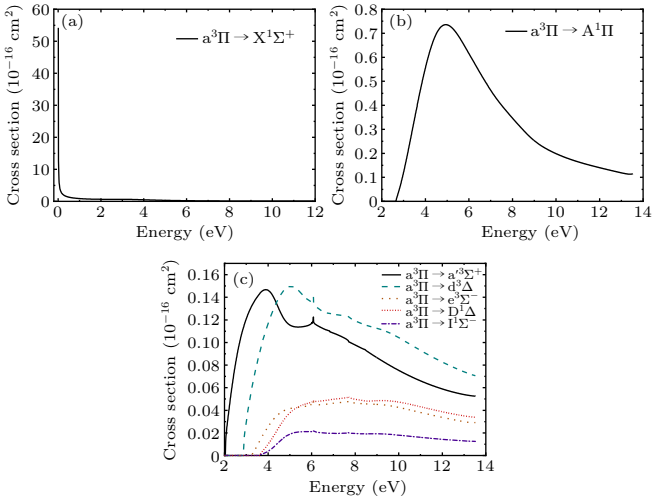


Fig. 2. De-excitation cross-sections for CO from the $a^3\Pi$ state to the (a) $X^1\Sigma^+$ state. Electronimpact excitation cross-sections for CO from the $a^3\Pi$ excited state to the (b) $A^1\Pi$, (c) $a'^3\Sigma^+$, $d^3\Delta$, $e^3\Sigma^-$, $I^1\Sigma^-$ and $D^1\Delta$ states.

4.2.2. The $a'^3\Sigma^+$ state

In general, the de-excitation cross-sections $a'^3\Sigma^+ \rightarrow X^1\Sigma^+$ and $a'^3\Sigma^+ \rightarrow a^3\Pi$ depicted in Figs. 3(a) and 3(b) show a decreasing trend as the incident electron energy increases. However, an exception is observed for the excitation cross-sections for $a'^3\Sigma^+ \rightarrow A^1\Pi$, $e^3\Sigma^-$, $I^1\Sigma^-$ and $D^1\Delta$ in Fig. 3(c), wherein there is an obvious peak at 11.26 eV. The cross-section peak of the $a'^3\Sigma^+ \rightarrow D^1\Delta$ transition is 1.32 times larger than that of the $a'^3\Sigma^+ \rightarrow I^1\Sigma^-$ transition. Meanwhile, it is worth mentioning that the electron-impact excitation processes leading from the $a'^3\Sigma^+$ state to $e^3\Sigma^-$ and $A^1\Pi$ metastable states show a low probability. The peak value of cross-sections for the transitions $a'^3\Sigma^+ \rightarrow D^1\Delta$ and $a'^3\Sigma^+ \rightarrow I^1\Sigma^-$ are approximately 3–17 times larger than those for the transitions $a'^3\Sigma^+ \rightarrow A^1\Pi$, $a'^3\Sigma^+ \rightarrow d^3\Delta$ and $a'^3\Sigma^+ \rightarrow e^3\Sigma^-$. It is justifiable to demonstrate that the cascade observed at $a'^3\Sigma^+$ predominantly arises from the $I^1\Sigma^-$ and $D^1\Delta$ states, while the influence of the $a^3\Pi$, $d^3\Delta$ and $e^3\Sigma^-$ states can be ignored. This explains the experimental error attributed to the cascade phenomenon.

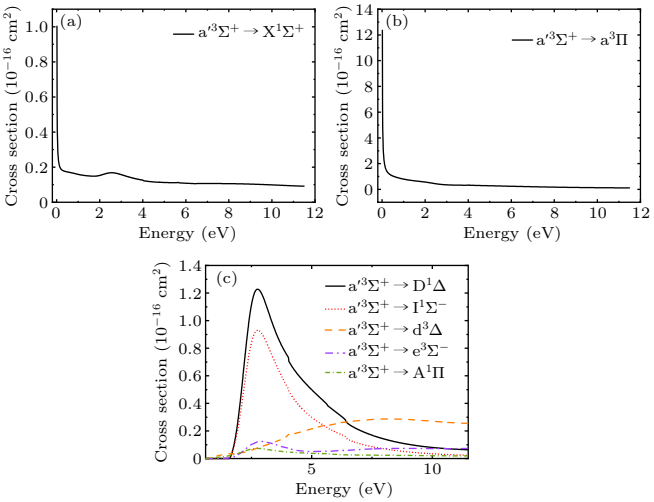


Fig. 3. De-excitation cross-sections for CO from the $a'^3\Sigma^+$ excited state to the (a) $X^1\Sigma^+$ and (b) $a^3\Pi$ states. Excitation cross-sections for CO from the $a'^3\Sigma^+$ excited state to the (c) $A^1\Pi$, $d^3\Delta$, $e^3\Sigma^-$, $I^1\Sigma^-$ and $D^1\Delta$ states.

4.2.3. The $A^1\Pi$ state

Figure 4(a) illustrates that the de-excitation cross-sections of $A^1\Pi \rightarrow X^1\Sigma^+$ generally show a decreasing trend as the incident electron energy increases, except for the slight changes observed at the peaks located at 10.89 eV, 12.54 eV, 13.28 eV and 14.15 eV. The electronic transition of $A^1\Pi \rightarrow a^3\Pi$ displays a distinct peak structure that exists at 11.21 eV. Moreover, the de-excitation integral sections all demonstrate a rapid and abrupt decrease during the initial phase of increasing electron energy. The electronic transition of $A^1\Pi \rightarrow a'^3\Sigma^+$ shows a relatively small cross-section, indicating its minimal contribution to the overall cross-sections. The electronic transitions of $A^1\Pi \rightarrow I^1\Sigma^-$ and $A^1\Pi \rightarrow D^1\Delta$ show similar characteristics in terms of shape and magnitude, both displaying two peaks. The initial broad peak ranges from approximately 10.50 eV to 11.00 eV, followed by a subsequent narrow peak at 14.15 eV. The transitions of $A^1\Pi \rightarrow d^3\Delta$ and $A^1\Pi \rightarrow e^3\Sigma^-$ that are shown in Fig. 4(c) represent the initial two electronic

excitation processes of the $A^1\Pi$ state. While these transitions share similar shapes, the former shows greater energy cross-sections within the range of 9.34 eV to 19.99 eV.

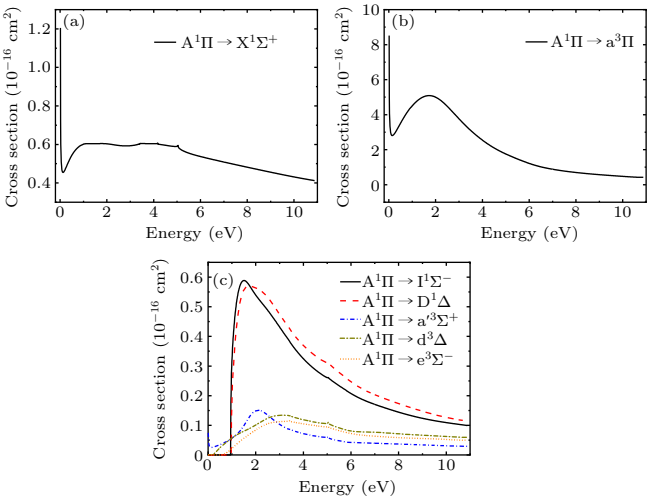


Fig. 4. De-excitation cross-sections for CO from the $A^1\Pi$ excited state to the (a) $X^1\Sigma^+$, (b) $a^3\Pi$ and (c) $a'^3\Sigma^+$ states. Electron impact excitation cross-sections for CO from the $A^1\Pi$ excited state to the (c) $d^3\Delta$, $e^3\Sigma^-$, $I^1\Sigma^-$ and $D^1\Delta$ states.

The excitation cross-sections of the $A^1\Pi$ state are depicted in Fig. 4(c), which is important and has not been previously addressed. It is reasonable to demonstrate that the cascade observed at the $A^1\Pi$ state is predominantly produced by $I^1\Sigma^-$ and $D^1\Delta$ states, thereby allowing us to ignore the influence of the $a'^3\Sigma^+$, $d^3\Delta$ and $e^3\Sigma^-$ states. The $I^1\Sigma^-$ and $D^1\Delta$ states have a more obvious effect on the experimental measurement of the fourth positive band system ($A^1\Pi \rightarrow X^1\Sigma^+$) of CO. This assists us to comprehend the experimental error resulting from the cascade when employing the electron beam excitation method to measure the fourth positive band system.

4.2.4. The $d^3\Delta$ state

Regarding the collision process from the excited state $d^3\Delta$ to the ground state $X^1\Sigma^+$, within the limited range of initial collision energy increase, the ICSs solely show a declining trend. The ICSs show a gradual decline after reaching their peak at 10.28 eV. Similarly, the cross-sections of $d^3\Delta \rightarrow A^1\Pi$ de-excitation display a sharp decrease within a limited range, followed by an initial increase and subsequent downward trend as the energy continues to rise. As depicted in Fig. 5(c), the de-excitation cross-sections of $d^3\Delta \rightarrow a'^3\Sigma^+$ demonstrate a pronounced decrease within a narrow range, accompanied by a gradual increase and subsequent decline in the higher-energy range. The electronic transitions of the $d^3\Delta \rightarrow X^1\Sigma^+$, $d^3\Delta \rightarrow A^1\Pi$ illustrated in Fig. 5(a) and $d^3\Delta \rightarrow a'^3\Sigma^+$ illustrated in Fig. 5(c) show significantly smaller cross-sections, indicating that these processes make a negligible contribution to the overall ICSs. The de-excitation cross-sections $d^3\Delta \rightarrow a^3\Pi$ depicted in Fig. 5(b) show a decrease as the incident electron energy increases. The electronic transitions $d^3\Delta \rightarrow e^3\Sigma^-$, $d^3\Delta \rightarrow I^1\Sigma^-$ and $d^3\Delta \rightarrow D^1\Delta$ illustrated in Fig. 5(c) demonstrate a notable similarity in shape, with a prominent peak observed within the energy range of 12.22 eV to 13.01 eV.

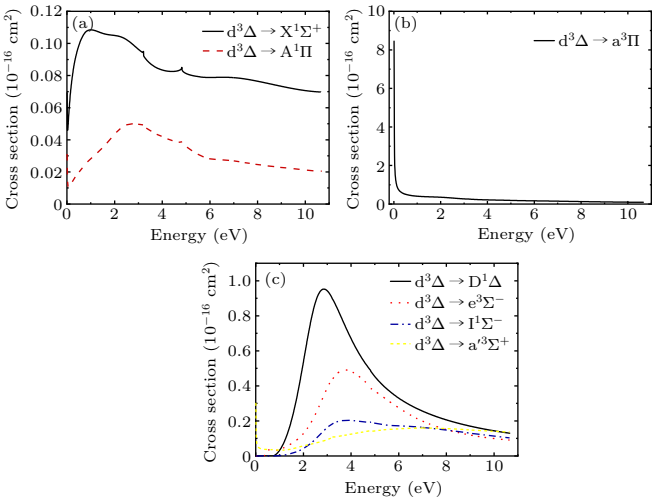


Fig. 5. De-excitation cross-sections for CO from the $d^3\Delta$ excited state to the (a) $X^1\Sigma^+$, $A^1\Pi$ (b) $a^3\Pi$ and (c) $a'^3\Sigma^+$ states. Electron impact excitation cross-sections for CO from the $d^3\Delta$ excited state to the (c) $e^3\Sigma^-$, $I^1\Sigma^-$ and $D^1\Delta$ states.

4.2.5. The $e^3\Sigma^-$, $I^1\Sigma^-$ and $D^1\Delta$ states

Figure 6 presents the de-excitation/excitation cross-sections from the $e^3\Sigma^-$, $I^1\Sigma^-$ and $D^1\Delta$ excited states to the other states. It is evident from Fig. 6 that the de-excitation cross-sections of $e^3\Sigma^- \rightarrow a^3\Pi$, $I^1\Sigma^- \rightarrow A^1\Pi$ and $D^1\Delta \rightarrow A^1\Pi$ generally decrease as the incident electron energy increases. Apart from the above mentioned de-excitation process, the remaining de-excitation processes depicted in Fig. 6

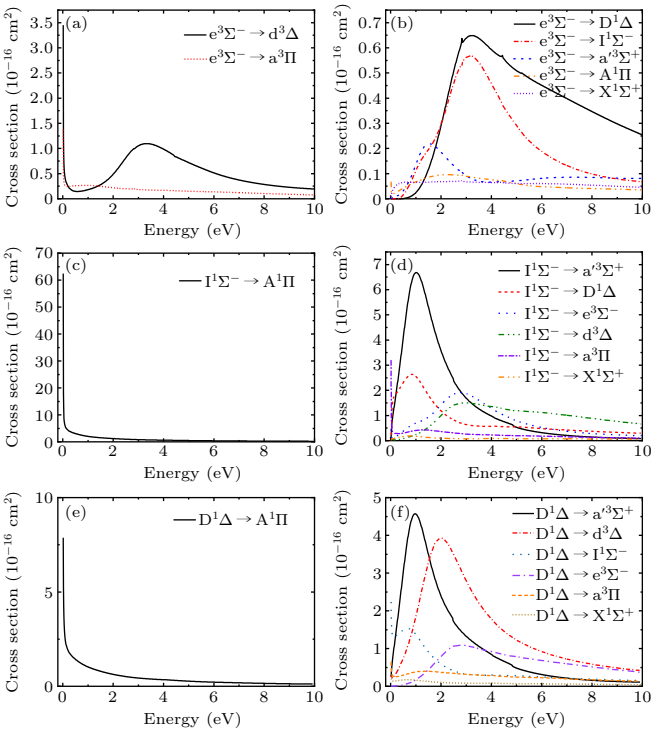


Fig. 6. Electron impact excitation and de-excitation cross-sections from the $e^3\Sigma^-$, $I^1\Sigma^-$ and $D^1\Delta$ excited states of CO to the other states.

demonstrate a gradual increase leading to a wide peak, with energy peaks centered between 9.71 eV and 13.71 eV. The cross-sections show a gradual decrease after the peak, which leads us to the assumption that resonance plays a role in the peak of the cross-sections.

5. Conclusion

The present study focuses on investigating and analyzing the scattering cross-sections of electron collisions with CO in both its ground state and excited metastable states utilizing the *R*-matrix method. The vertical excitation energies are in good agreement with the previous reference values. The study investigates the cross-sections associated with electron-impact (de-)excitation from the metastable states of CO, marking the first instance of such an investigation. In addition, we report, for the first time, the impact of cascade effects by comprehensively calculating the excitation of the $a^3\Pi$, $a'^3\Sigma^+$ and $A^1\Pi$ states. Notably, the higher-lying single states ($I^1\Sigma^-$ and $D^1\Delta$) of CO play a crucial role in the cascade process towards CO $a'^3\Sigma^+$ and $A^1\Pi$ states.

Acknowledgment

Project supported by the National Natural Science Foundation of China (Grant No. 11974253).

References

[1] Campbell L, Allan M and Brunger M J 2011 *J. Geophys. Res. Space Phys.* **116** A09321
[2] Wang T and Cheng Q 2001 *Opt. Laser Technol.* **33** 475
[3] Gorse C, Cacciatore M and Capitelli M 1984 *Chem. Phys.* **85** 165
[4] Chung S and Lin C C 1974 *Phys. Rev. A* **9** 1954
[5] Sun Q, Winstead C and McKoy V 1992 *Phys. Rev. A* **46** 6987
[6] Morgan L A and Tennyson J 1993 *J. Phys. B: At. Mol. Opt. Phys.* **26** 2429
[7] Itikawa Y 2015 *J. Phys. Chem. Ref. Data* **44** 013105
[8] Zawadzki M, Khakoo M A, Voorneman L, Ratkovic L, Masin Z, Houfek K, Dora A, Laher R and Tennyson J 2020 *J. Phys. B: At. Mol. Opt. Phys.* **53** 165201
[9] Ajello J M 1971 *J. Chem. Phys.* **55** 3158
[10] LeClair L R, Brown M D and McConkey J W *J. Chem. Phys.* **189** 769
[11] Furlong J M and Newell W R 1996 *J. Phys. B: At. Mol. Opt. Phys.* **29** 331
[12] Bardsley J N and Mandl F 1968 *Rep. Prog. Phys.* **31** 471
[13] Dora A and Tennyson J 2020 *J. Phys. B: At. Mol. Opt. Phys.* **53** 195202
[14] Mašín Z, Benda J, Gorfinkiel J D, Harvey A G and Tennyson J 2020 *Comput. Phys. Commun.* **249** 107092
[15] Werner H J, Knowles P J, Knizia G, Manby F R and Schütz M 2012 *Wiley Interdiscip. Rev. Comput. Mol. Sci.* **2** 242
[16] Tennyson J 2010 *Phys. Rep.* **491** 29
[17] Nielsen E S, Jorgensen P and Oddershede J 1980 *J. Chem. Phys.* **73** 6238
[18] Tilford S G and Simmons J D 1972 *J. Phys. Chem. Ref. Data* **1** 147
[19] Zobel J, Mayer U, Jung K and Ehrhardt H 1996 *J. Phys. B: At. Mol. Opt. Phys.* **29** 813
[20] Huo W M 1966 *J. Chem. Phys.* **45** 1554
[21] Faure A, Gorfinkiel J D, Morgan L A and Tennyson J 2002 *Comput. Phys. Commun.* **144** 224